Cell Reports
Article

Differential Effects of EGFL6 on Tumor versus Wound Angiogenesis

Kyunghee Noh,[1,4,16] Lingegowda S. Mangala,[1,3,16] Hee-Dong Han,[5,16] Ningyan Zhang,[6] Sunila Pradeep,[1,7] Sherry Y. Wu,[1] Shaolin Ma,[1] Edna Mora,[8,9,10] Rajesha Rupaimoole,[1] Dahai Jiang,[1,3] Yunfei Wen,[1] Mian M.K. Shahzad,[1] Yasmin Lyons,[1] MinSoon Cho,[11] Wei Hu,[1] Archana S. Nagaraja,[1] Monika Haemmerle,[1] Celia S.L. Mak,[1] Xiuhui Chen,[1] Kshipra M. Gharpure,[1] Hui Deng,[6] Wei Xiong,[6] Charles V. Kingsley,[12] Jinsong Liu,[13] Nicholas Jennings,[1] Michael J. Birrer,[14] Richard R. Bouchard,[12] Gabriel Lopez-Berestein,[2,3,15] Robert L. Coleman,[1] Zhiqiang An,[6] and Anil K. Sood[1,2,3,17,*]

[1]Department of Gynecologic Oncology and Reproductive Medicine, The University of Texas MD Anderson Cancer Center, Houston, TX 77030, USA
[2]Department of Cancer Biology, The University of Texas MD Anderson Cancer Center, Houston, TX 77030, USA
[3]Center for RNA Interference and Non-Coding RNA, The University of Texas MD Anderson Cancer Center, Houston, TX 77030, USA
[4]Gene Therapy Research Unit, Korea Research Institute of Bioscience and Biotechnology, Daejeon, Republic of Korea
[5]Department of Immunology, School of Medicine, Konkuk University, Chungju 380-701, South Korea
[6]Texas Therapeutics Institute, Brown Foundation Institute of Molecular Medicine, The University of Texas Health Science Center at Houston, Houston, TX 77030, USA
[7]Department of Obstetrics and Gynecology, Medical College of Wisconsin, Milwaukee, WI 53226, USA
[8]Department of Surgery, University of Puerto Rico, San Juan 00936, Puerto Rico
[9]University of Puerto Rico Comprehensive Cancer Center, San Juan 00936, Puerto Rico
[10]Department of Surgical Oncology, The University of Texas MD Anderson Cancer Center, Houston, TX 77584, USA
[11]Department of Benign Hematology, The University of Texas MD Anderson Cancer Center, Houston, TX 77030, USA
[12]Department of Imaging Physics, The University of Texas MD Anderson Cancer Center, Houston, TX 77030, USA
[13]Department of Pathology, The University of Texas MD Anderson Cancer Center, Houston, TX 77030, USA
[14]University of Alabama Comprehensive Cancer Center, Birmingham, AL 35294, USA
[15]Department of Experimental Therapeutics, The University of Texas MD Anderson Cancer Center, Houston, TX 77030, USA
[16]These authors contributed equally
[17]Lead Contact
*Correspondence: asood@mdanderson.org
https://doi.org/10.1016/j.celrep.2017.11.020

SUMMARY

Angiogenesis inhibitors are important for cancer therapy, but clinically approved anti-angiogenic agents have shown only modest efficacy and can compromise wound healing. This necessitates the development of novel anti-angiogenesis therapies. Here, we show significantly increased EGFL6 expression in tumor versus wound or normal endothelial cells. Using a series of *in vitro* and *in vivo* studies with orthotopic and genetically engineered mouse models, we demonstrate the mechanisms by which EGFL6 stimulates tumor angiogenesis. In contrast to its antagonistic effects on tumor angiogenesis, EGFL6 blockage did not affect normal wound healing. These findings have significant implications for development of anti-angiogenesis therapies.

INTRODUCTION

Angiogenesis is essential for many physiological and pathological processes, such as embryogenesis, pregnancy, wound healing, tumor growth, and metastasis (Bergers and Benjamin, 2003; Breier, 2000; Tonnesen et al., 2000; Eming et al., 2007; Gressett and Shah, 2009; Shord et al., 2009). To date, multiple anti-angiogenesis drugs (e.g., bevacizumab) have been developed and tested. Although modest efficacy has been noted with this class of drugs against many cancers, specific adverse effects such as hypertension and impaired wound healing have been a significant concern (Gressett and Shah, 2009; Shord et al., 2009; Koskas et al., 2010). Therefore, we asked whether targets unique for tumor angiogenesis could be identified and used for therapeutic development. To address this question, we carried out a series of experiments to identify targets that are differentially expressed in tumor angiogenesis. Among these, EGFL6 (epidermal growth factor [EGF]-like domain multiple 6) was found to be highly expressed in tumor-associated endothelial cells compared to normal ovarian and wound-associated endothelial cells. EGFL6, also called MAEG, is a secreted protein that belongs to the EGF repeat superfamily. EGFL6 was mapped to the human Xp22 chromosome and has been shown to be expressed during early development, mainly in fetal tissues of lung, skin, umbilical cord, liver or spleen, and placenta, but not in normal adult tissues (Yeung et al., 1999; Buchner et al., 2000). Although it has been shown to be expressed in some tumors (Wang et al., 2012; Buckanovich et al., 2007), its unique role in tumor angiogenesis identifies it as an important target that does not impair wound healing.

RESULTS

EGFL6 Is Upregulated in Tumor-Associated Endothelial Cells

To identify candidate targets that are important for tumor angiogenesis, but not wound healing, we first isolated endothelial cells from 10 high-grade serous (ovarian) cancers (HGSCs), 5 normal ovarian tissues, and 7 healing wound patient samples. RNA was isolated and subjected to genomic analyses. We found that 375 genes were upregulated in HGSC endothelial cells compared with those from normal ovarian and healing wound tissues (Figure 1A). Among these genes, *EGFL6* showed the highest differential expression (52.63-fold higher) in tumor endothelial cells compared with normal ovarian endothelial cells (Figure 1B). Expression of EGFL6 and VEGF in ovarian patient samples was examined. As expected, VEGF was expressed in ovarian cancer tissues and in healing wounds (Figure S1A), but EGFL6 was expressed mainly in tumor-associated endothelial cells (Figure 1C). To validate the microarray results, we isolated endothelial cells from an independent cohort of normal ovarian, HGSC, and wound tissues and examined *EGFL6* expression using qRT-PCR. *EGFL6* was predominantly expressed in tumor endothelial cells, but not in normal ovary or wound endothelial cells (Figure 1D).

Next, we studied the biological implications of EGFL6 upregulation in tumor endothelial cells. To investigate the biological functions of EGFL6 in tumor angiogenesis, RF24 cells were treated with *EGFL6* small interfering RNA (siRNA). There was more than 80% knockdown in EGFL6 protein levels within 72 hr compared with non-targeting siRNA in control cells (Figure S1B). *EGFL6* siRNA-treated cells showed significantly reduced tube formation and migration compared to control siRNA-treated cells (Figures S1C and S1D).

EGFL6 Silencing Did Not Affect Wound Healing in Mice

Because EGFL6 expression was not increased in wound endothelial cells, we next asked whether *EGFL6* silencing would have any effect on wound healing. To address this question, we used a wound healing mouse model. As expected, treatment with DC101 (VEGFR2-blocking antibody) (Witte et al., 1998; Zhu et al., 1998) resulted in significant impairment of wound healing (Figure 2A; Figure S2A). To test the potential effects of EGFL6 on tumor growth and wound healing, we examined *EGFL6* mRNA levels in ovarian cancer cells (Figure S2B). We used our well-characterized chitosan (CH) nanoparticle delivery system that is highly efficient for delivery to tumor vasculature (Figure S2C) (Lu et al., 2010; Masiero et al., 2013; Krzeszinski et al., 2014). Mouse *EGFL6* (m*EGFL6*) siRNA-CH had no significant effect on wound healing compared with control siRNA-CH (Figure 2B; Figure S2D). However, m*EGFL6* siRNA-CH-treated animals had significant reduction in SKOV3ip1 ovarian tumor burden (Figures 2C–2E). *EGFL6* gene silencing resulted in significant reduction in proliferation and tumor microvessel density (Figure S2E). As shown in Figures S2F and S2G, treatment of SKOV3ip1 tumor-bearing animals with m*EGFL6* siRNA alone and with a combination of mouse and human *EGFL6* siRNA resulted in significant reduction in tumor growth compared to controls. However, treatment with human *EGFL6* siRNA alone did not affect tumor growth, indicating that EGFL6 from endothelial cells is more decisive for tumor growth and angiogenesis (Figure S2H). A major difference between tumor and wound is the extent of hypoxia (Peng et al., 2012; Carmeliet and Jain, 2000; Schäfer and Werner, 2008). Given the differences in EGFL6 expression between tumor and wound endothelial cells, we asked whether hypoxia could be an important factor in regulating EGFL6 levels. To address this question, we created hindlimb ischemia on mice by ligating the femoral artery on the hindlimb of the mouse (Figure 2F) (Krishna et al., 2016). As shown in Figure 2G, ischemic tissues showed significant increase in EGFL6 levels in endothelial cells. Blood flow was recovered by 96 hr after ligation of the femoral artery.

TWIST1 Enhances EGFL6 for Hypoxia-Triggered Angiogenesis

To identify potential mechanisms of EGFL6 regulation in the tumor microenvironment, we next investigated EGFL6 transcriptional activity. Under hypoxia, EGFL6 promoter activity was significantly increased compared with levels under normoxia (Figure 3A). Upon promoter analysis, TWIST1 transcription factor was predicted to bind to the EGFL6 promoter (Figure S3A). EGFL6 transcriptional activity levels were similarly increased with ectopic expression of TWIST1, supporting a link between TWIST1 and EGFL6 (Figure 3B). Treatment of cells with $CoCl_2$, a HIF1-α stabilizer, also resulted in increased *EGFL6* and *TWIST1* levels (Figure 3C).

Next, we ectopically expressed *TWIST1* in RF24 endothelial cells and measured *EGFL6* levels. We found a significant increase in *EGFL6* levels in endothelial cells with elevated *TWIST1* compared with control cells (Figure 3D). Moreover, we silenced *TWIST1* with siRNA, and *EGFL6* levels did not increase under hypoxia conditions following *TWIST1* silencing (Figure S3B). Upon chromatin immunoprecipitation (ChIP) analysis with anti-TWIST1 antibody, the binding of TWIST1 to the *EGFL6* promoter region was significantly higher under hypoxic versus normoxic conditions (Figure 3E). Because EGFL6 expression was enhanced under hypoxic conditions, we next asked whether increased EGFL6 levels contribute to survival of endothelial cells under hypoxic conditions. To address this question, we silenced *EGFL6* in RF24 cells under hypoxia using *EGFL6* siRNA and determined the percentage of cell death. As shown in Figure 3F, almost 50% of cells survived the hypoxic conditions, even after 5 days, compared with those under normoxic conditions. In contrast, *EGFL6* gene silencing under hypoxia resulted in >75% cell death.

EGFL6-Mediated Tie2/PI3K/AKT Signaling

To understand the signaling events downstream of EGFL6, we conducted reverse phase protein array (RPPA) analyses of EGFL6-treated RF24 endothelial cells and untreated control cells. EGFL6-treated endothelial cells showed activation of phosphatidylinositol 3-kinase (PI3K) and AKT signaling (Figure 4A; Figure S4A). To validate these results, we treated RF24 endothelial cells with EGFL6 and examined them for AKT and PI3K signaling (Figure 4B; Figure S4B). EGFL6-treated RF24 cells showed increased expression of p-PI3K and pAKT compared with untreated cells. The migration (Figure S4C) and

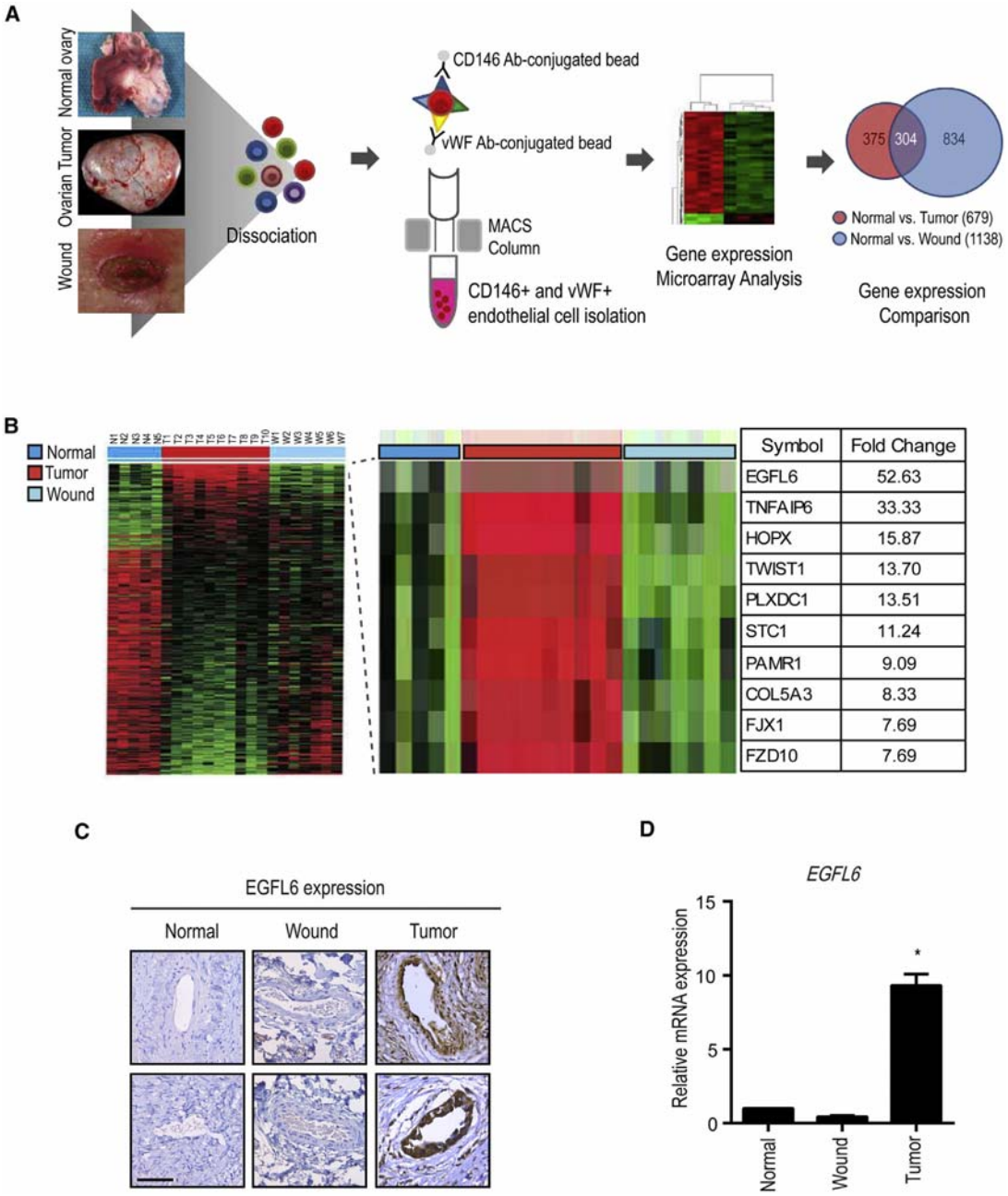

Figure 1. EGFL6 Is Upregulated in Tumor-Associated Endothelial Cells but Not in Normal Ovary and Healing Wound Tissues

(A) Human normal ovary, ovarian tumor, and healing wound tissues were dissociated, and isolated endothelial cells and samples were processed for microarray.

(B) Gene microarray of endothelial cells from normal ovary, healing wound tissue, and ovarian tumor-associated endothelial cells.

(C) Expression of EGFL6 in human normal ovary, wound, and ovarian tumor samples. Representative images were taken from different samples. Scale bar, 100 μm.

(D) Validation of gene microarray data using qPCR (normal ovary, n = 5; ovarian tumor, n = 10; wound, n = 7). Validation error bar indicates SEM. *$p < 0.05$ versus normal.

See also Figure S1.

tube formation (Figure S4D) of RF24 cells increased significantly after treatment with EGFL6, and these EGFL6-induced functions were completely blocked in the presence of a PI3K inhibitor, suggesting the key involvement of PI3K signaling. To identify candidate proteins involved in EGFL6-mediated AKT activation, we used a phospho-receptor tyrosine kinase (RTK) array and found activation of 3 RTKs, including insulin growth factor 1R (IGF-1R), EGF receptor (EGFR), and Tie2 (Figure S4E). We confirmed these

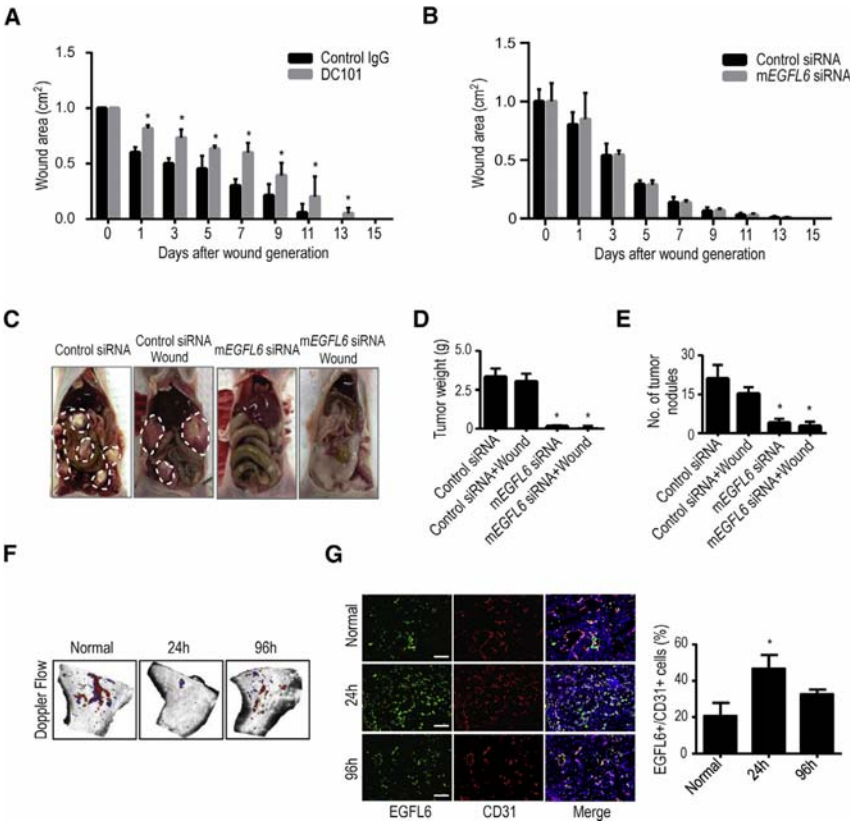

Figure 2. Effect of *EGFL6* Silencing on Tumor Growth in Orthotopic Ovarian Cancer Mouse Models

(A) Graph of wound area on mice treated with either control IgG antibody or DC101 (anti-VEGFR2) quantified on days 0 through 15 after a skin excision wound (n = 10 mice per group). *p < 0.05 versus control IgG.

(B) One day after SKOV3ip1 tumor cell injection, a wound was created on the dorsal side of the mice. Animals were treated with either control siRNA-CH or m*EGFL6* siRNA-CH. The graphical depiction shows wound areas quantified on days 0 through 15 after skin excision wound.

(C–E) Effect of m*EGFL6* silencing on tumor growth (C); representative images of tumor burden. Tumor weights are shown in (D), and numbers of tumor nodules are shown in (E) (n = 10 mice per group. *p < 0.05 versus control siRNA.

(F) Hindlimb ischemia. After arterial ligation, mice were separated into 3 groups (n = 5 mice per group): normal; ischemia, 24 hr; and 96 hr. Blood flow was monitored before and after femoral artery ligation with serial color Doppler. At each time point, tissue was harvested and frozen so that immunofluorescence staining could be performed.

(G) EGFL6 expression was increased in endothelial cells in the ischemic (hypoxic) condition compared with the normal conditions. *p < 0.05 versus normal.

Error bars indicate SEM. See also Figure S2.

results in EGFL6-treated RF24 cells using western blot analysis. As shown in Figure 4C, only Tie2 was activated in EGFL6-treated cells. EGFL6 contains Arg-Gly-Asp (RGD) motifs that can bind to integrins (Chim et al., 2011).

To gain insight into the mechanisms through which EGFL6 promotes Tie2 and αVβ3 or α5β1 binding capacity, we examined which integrins could bind to the Tie2 receptor. The potential interaction between the α5β1 integrin and the Tie2 receptor was confirmed by co-immunoprecipitation in the presence of EGFL6 (Figure 4D). Tie2 is broadly expressed on the membrane in cells. After stimulation with EGFL6, we tested whether it could be activated in the cell membrane. We determined Tie2 and AKT activation levels in the cytosolic and membrane fractions. Activation of Tie2 was substantially enhanced in EGFL6-stimulated cell membrane fractions (Figure 4E).

We next examined the effect of silencing *integrins* and *Tie2* on EGFL6-induced angiogenesis in RF24 cells. Silencing Integrin *β1* or *Tie2* using specific siRNA resulted in 80%–90% reduction of the gene expression and pAKT level (Figure 4F). As shown in Figures 4G and 4H, silencing of Integrin *β1* or *Tie2* significantly reduced both tube formation and migration. The addition of EGFL6 after silencing of these two components did not rescue either of these functions. We also determined the interaction of EGFL6 with integrins using a RGD-blocking peptide and evaluated its effects on EGFL6-mediated functions. As shown in Figures 4I–4K, endothelial cells treated with RGD-blocking peptide showed significant reduction in tube formation and migration compared with EGFL6-treated cells. Collectively, these data indicate that EGFL6 regulates Tie2/AKT signaling through α5β1 integrin to promote endothelial cell migration and tube formation. However, *EGFL6* silencing in the SKOV3ip1 cancer cells did not affect Tie2/AKT signaling (Figure S4F). Similarly, EGFL6-treated RMG2 tumor cells did not show significant changes in PI3K/AKT signaling (Figure S4G).

EGFL6 Antibody Blocks Tumor Angiogenesis

Given the robust anti-angiogenesis effects of silencing EGFL6, we next aimed to develop neutralizing antibodies and tested their effects on angiogenesis. To identify monoclonal antibodies (mAbs) targeting EGFL6, we screened a large panel of mAbs (>3,000) produced from single memory B cells isolated from peripheral blood mononuclear cells (PBMCs) of a rabbit immunized with human EGFL6, and more than 300 clones showed high EGFL6 binding by ELISA (Figures S5A and S5B). Two functional mAbs (mAb 93 and mAb 135) were characterized further (Figures S5A–S5C) and used for both *in vitro* and *in vivo* experiments. Figure 5A shows concentration dependence of high-affinity binding on human EGFL6 by the two lead mAbs. Kinetic binding constants (dissociation constant [K_D]) of the two mAbs to human EGFL6 were 1.89 nM for mAb 93 and 2.19 nM for mAb 135 (Figure S5D).

As shown in Figure 5B, treatment of endothelial cells with EGFL6-blocking mAb 93 and mAb 135 resulted in reduction in expression of both phosphorylated Tie2 and AKT (Figure S5E). We also examined potential effects of these antibodies on

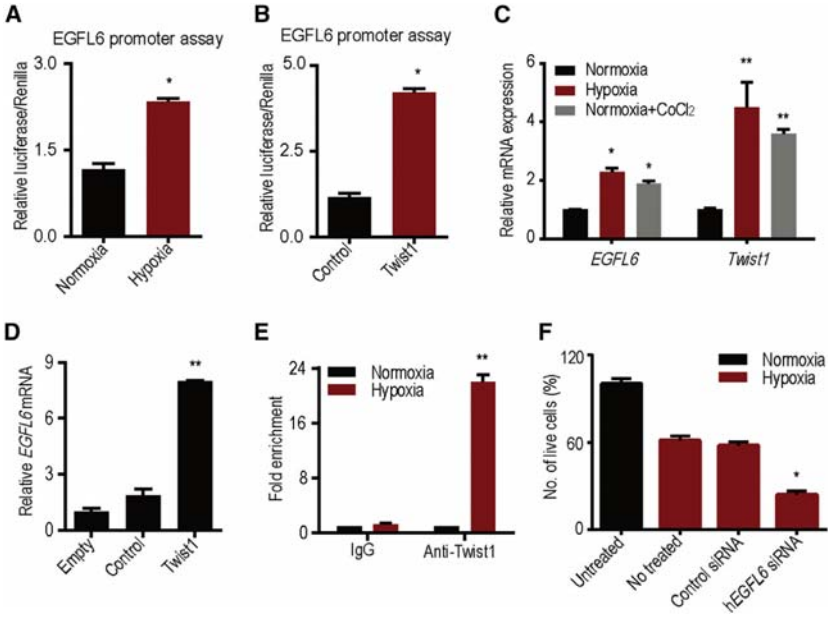

Figure 3. TWIST1 Induces *EGFL6* Expression under Hypoxia

(A) *EGFL6* promoter reporter analysis under normoxia and hypoxic conditions.

(B) *TWIST1* ectopic expression increases *EGFL6* transcription activity.

(C) Increase in *TWIST1* and *EGFL6* expression in hypoxia and $CoCl_2$ treatment.

(D) Ectopic expression of *TWIST1* increases *EGFL6* expression in RF24 cells.

(E) ChIP analysis of TWIST1 binding to the *EGFL6* promoter region in hypoxia compared with normoxia. Cross-linked chromatin from RF24 cells was incubated in a hypoxia chamber for 48 hr and immunoprecipitated with TWIST1 or IgG control antibodies. The input and immunoprecipitated DNA was subjected to PCR using primers corresponding to the base pairs upstream of the *EGFL6* transcription start site.

(F) *EGFL6* gene silencing using siRNA leads to increased cell death in the hypoxia condition (n = 3). $^{**}p < 0.005$, $^{*}p < 0.05$. See also Figure S3.

wound healing. EGFL6-neutralizing antibody had no effect on wound healing *in vivo* (Figure 5C). EGFL6-mediated functional effects on tube formation (Figure 5D) and migration (Figure 5E) were blocked by EGFL6-targeted antibodies.

Next, we determined whether anti-EGFL6 antibodies could block tumor angiogenesis *in vivo*. Human ovarian cancer (SKOV3ip1) or breast cancer (MDA-MB-231) tumor-bearing mice (n = 10 mice per group) were treated with either control or anti-EGFL6 antibodies. After 5 weeks of treatment, tumors were harvested and checked for anti-tumor and anti-angiogenic effects. Anti-EGFL6 antibodies displayed potent anti-tumor activity compared to control antibody. Treatment with either anti-EGFL6 mAb 93 or anti-EGFL6 mAb 135 resulted in significant reduction in tumor growth (Figure 5F; Figure S5F). Tumors treated with the EGFL6-targeted antibody showed decreased cell proliferation and microvessel density (MVD) compared with those from the control antibody-treated groups (Figure 5G; Figure S5G).

EGFL6 Silencing Inhibits Tumor Growth and Angiogenesis

To determine the role of EGFL6 during tumor development, conditional EGFL6$^{fl/fl}$ mice were generated and crossed with *Tie2-Cre* transgenic mice, thereby targeting cre recombinase in endothelial cells (Figure S6A). We isolated endothelial cells from wild-type (WT) and *Tie2;EGFL6* knockout (KO) mice (Figure S6B). As shown in Figure S6C, *EGFL6* mRNA was not expressed in *EGFL6* KO endothelial cells. There was no significant difference observed in either the weight or the morphology of organs such as lung, liver, kidney, spleen, and heart in WT and KO mice (Figures S6D and S6E). For testing the role of EGFL6 expression under ischemic conditions, we created hindlimb ischemia on WT and KO mice by ligation of the femoral artery in the hindlimb of mice (Figure S6F). Blood flow was recovered by 96 hr after ligation of femoral artery in both WT and KO mice. To identify the role of EGFL6 in tumor endothelial cells, we injected WT and KO mice with murine ID8 ovarian cancer or murine E0771 breast cancer cells. We detected EGFL6 expression in the tumor vasculature in WT mice, but not in KO mice (Figure 6B). We compared the tumor burden in WT and KO mice and found that tumor weight in KO mice was significantly lower compared to that of WT mice (Figures 6A and 6C; Figure S6G). Furthermore, tumor cell proliferation and MVD were lower in tumor-bearing KO mice than in tumor-bearing WT mice (Figures 6D and 6E).

To evaluate the potential clinical relevance of EGFL6, we examined 130 HGSCs. Increased vascular expression of EGFL6 was noted in 73% of the samples (Figure 6F). Increased expression of EGFL6 in tumor vasculature was significantly associated with high-stage disease ($p < 0.002$) (Table S1) and was related to poor overall survival ($p < 0.001$) (Figure 6G).

DISCUSSION

Our findings identify major differences in tumor compared to wound angiogenesis. Among these, EGFL6 was found to be increased in tumor endothelial cells in response to hypoxia-mediated TWIST1 and AKT pathway activation (Figure S6H). Based on these data, we generated EGFL6-targeted mAbs that bind effectively to EGFL6 with high affinity and block tumor angiogenesis without affecting wound healing.

VEGF has been recognized as a key target for anti-angiogenesis therapy. However, current angiogenesis inhibitors can cause intolerable adverse effects, including bleeding and impaired wound healing. The most broadly used anti-angiogenesis drug is bevacizumab, a monoclonal antibody that blocks the activity of VEGF-A (Ferrara and Kerbel, 2005). Given the effects of anti-VEGF drugs on wound healing, they cannot be safely

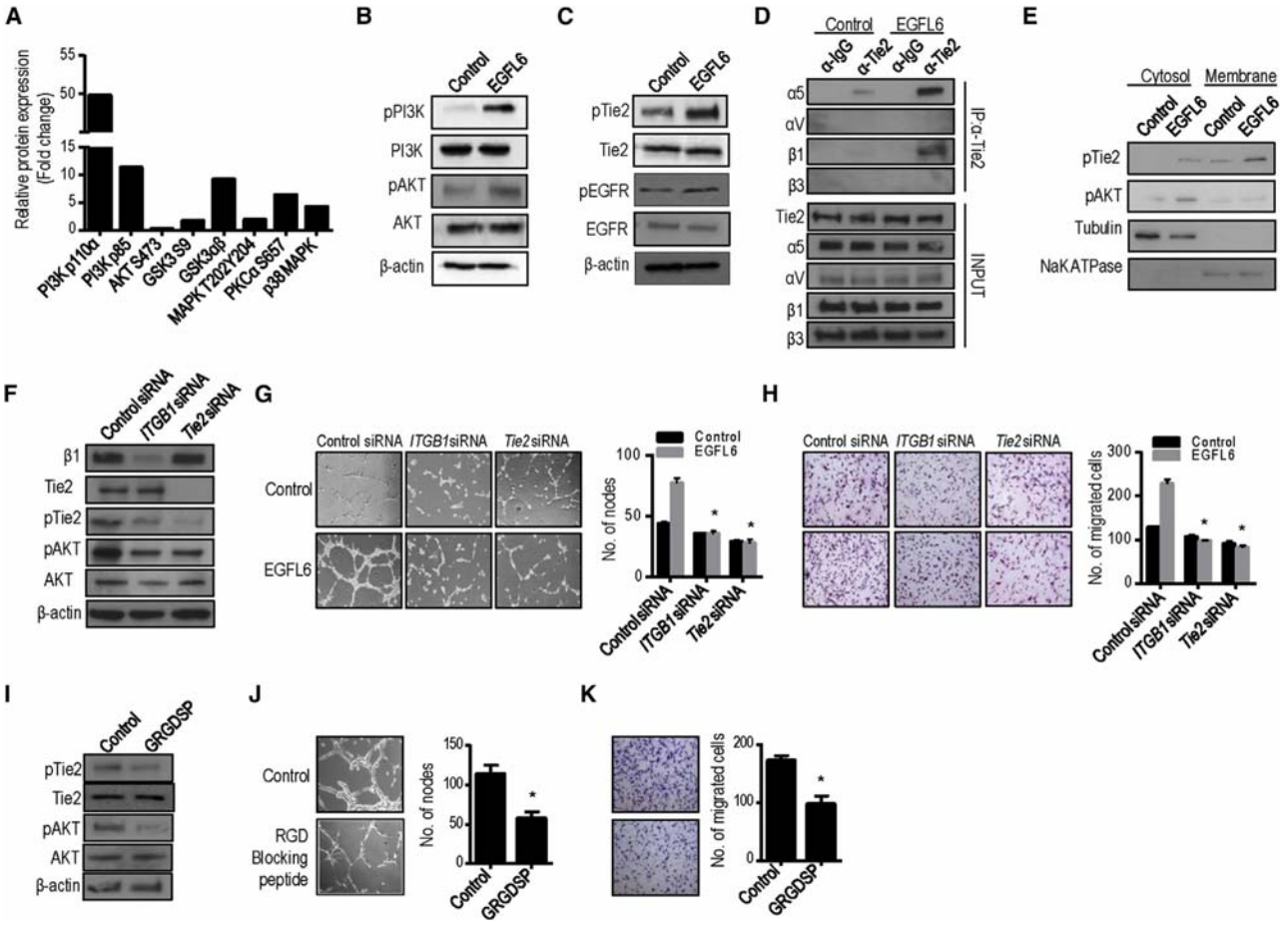

Figure 4. Treatment of EGFL6 Activates PI3K/AKT Signaling

(A) Expression level change in selected proteins after normalization by RPPA analysis.

(B and C) Western blotting of EGFL6-mediated activation of PI3K/AKT signaling (B), Tie2, and EGFR signaling (C).

(D) RF24 cells treated with control (PBS) or EGFL6. Extracts were subjected to anti-Tie2 immunoprecipitation (IP) and integrin α5, αV, β1, and β3 detected by immunoblotting.

(E) Expression level of pTie2 and pAKT in cytosol and membrane fractions with control (PBS) and EGFL6 treatment. αβ-tubulin (Tubulin) was used as the internal control of the cytosolic fraction; NaK ATPase was used as the membrane marker.

(F) Silencing of *Integrin β1* (ITGB1) and *Tie2* using specific siRNAs decreases Tie2 and AKT signaling.

(G and H) Silencing of *Integrin β1* (ITGB1) and *Tie2* decreases EGFL6-mediated tube formation (G) and migration (H) in endothelial cells. *$p < 0.05$ versus control siRNA.

(I–K) RGD-blocking peptide decreases Tie2/AKT activation (I), tube formation (J), and migration (K) ($n = 3$). *$p < 0.05$ versus control.

See also Figure S4.

used peri-operatively. Therefore, identifying targets that have differential expression between normal and tumor angiogenesis could be highly valuable for improving the efficacy and safety of anti-angiogenesis approaches. The observed effects of EGFL6-blocking mAbs in impairing tumor angiogenesis and growth without affecting wound healing indicate this to be such a target.

EGFL6 is a member of the EGF domain containing the EGF repeat superfamily of proteins. It is known to be expressed in some tissues such as benign meningioma, mouse microvascular endothelial cells, and ovarian and oral squamous cell carcinomas (Bai et al., 2016; Chim et al., 2011; Chuang et al., 2017; Oberauer et al., 2010; Buckanovich et al., 2007). It is also known to be expressed in some fetal tissues (Yeung et al., 1999). In a recent report, EGFL6 was found to be a stem cell regulatory factor in ovarian cancer and regulate ALDH+ ovarian cancer stem-like cells via the SHP2/ERK signaling pathway. Moreover, vascular EGFL6 expression was found to mediate ovarian tumor growth (Bai et al., 2016). Although several signaling pathways are potentially activated in various tissues by EGFL6, we provide an understanding of EGFL6 function in triggering integrin/Tie2/AKT signaling, which is a potent angiogenesis-regulating signaling axis. EGFL6 levels in tumor endothelial cells were found to be regulated by TWIST1.

EGFL7, another EGF-like family protein, is also highly expressed in vasculature (Schmidt et al., 2007). It has been reported that delayed development of vasculature in organs was

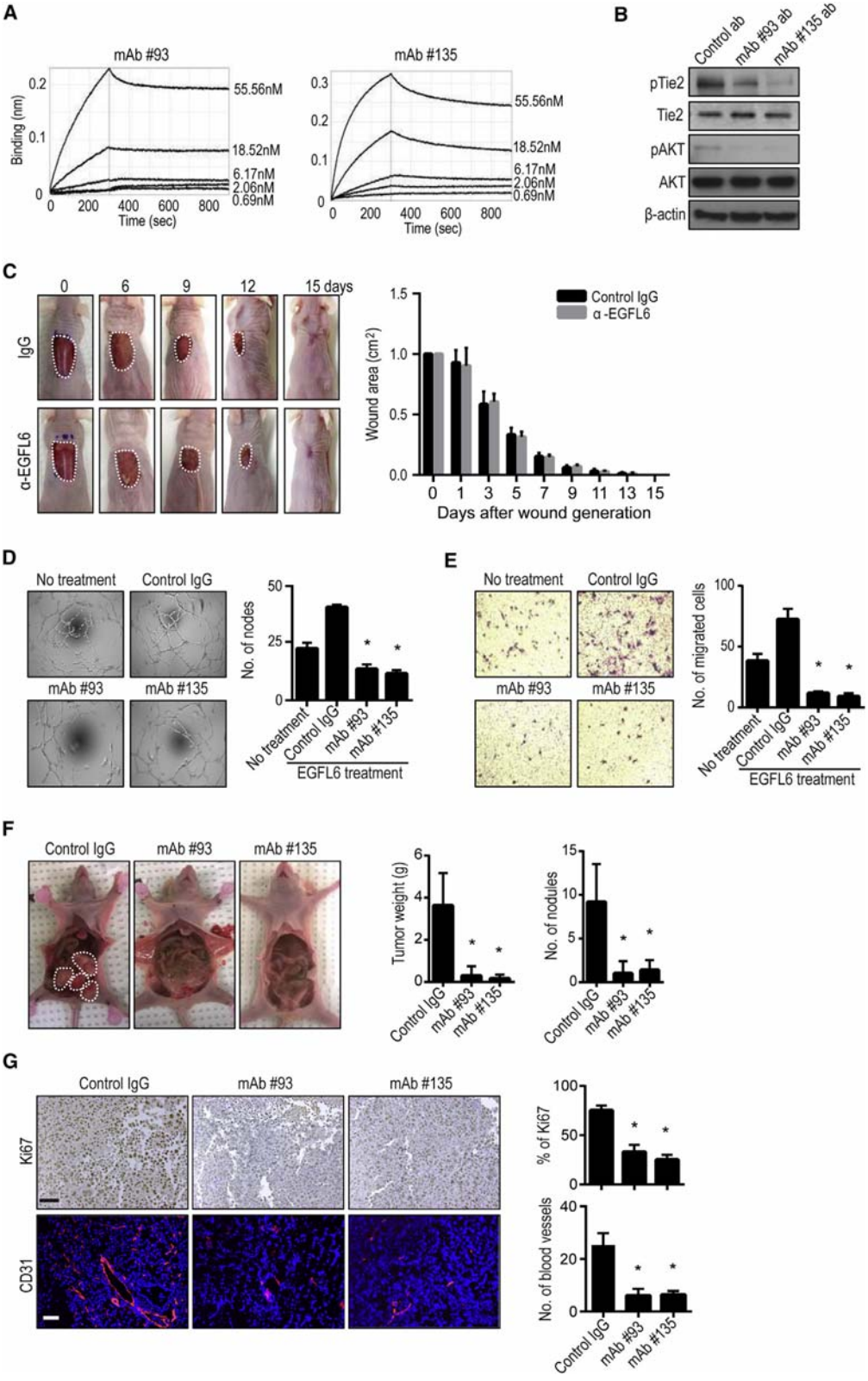

(legend on next page)

found in EGFL7 KO mice due to inhibition of angiogenesis by blocking autocrine Notch signaling in vasculature (Nichol and Stuhlmann, 2012). Moreover, the Mutant Mouse Resource and Research Center (MMRRC) has reported that female EGFL6 KO mice (deleted exon-1) are embryonic lethal. However, mechanisms underlying expression of EGFL6 in various tissues and embryonic lethality are not fully understood. Here, we generated endothelial cell-specific KO mice with Tie2-cre mice, which was not associated with lethality in both female and male mice. In addition, all organs tested were morphologically normal. Although many angiogenic factor KO mice are embryonic lethal, the EGFL6;Tie2 KO mice are viable and could be a powerful tool for biological studies. In summary, we have demonstrated that EGFL6 levels are selectively increased in tumor endothelial cells and represent an attractive therapeutic target for inhibiting ovarian and other cancers while mitigating off-target effects and toxicity.

EXPERIMENTAL PROCEDURES

Cell Lines and Culture

Human breast cancer cell line MDA-MB-231 and human epithelial ovarian cancer cell lines SKOV3ip1, HeyA8, A2780, OVCAR5, OVCAR8, RMG2, and IGROV1 were maintained as described previously (Pradeep et al., 2015). Human immortalized umbilical endothelial cells (RF24) and human dermal microvascular endothelial cells were grown in minimum essential medium (MEM) medium with supplements (sodium pyruvate, non-essential amino acids, MEM vitamins, and glutamine; Life Technologies, Grand Island, NY). The derivation and characterization of the mouse ovarian endothelial cells has been described previously (Langley et al., 2003). Cell cultures were maintained at 37°C in a 5% CO_2 incubator with 95% humidity. For *in vivo* injections, cells were trypsinized and centrifuged at 1,200 rpm for 5 min at 4°C, washed twice with PBS, and reconstituted in serum-free Hank's balanced salt solution (Life Technologies). Only single-cell suspensions with more than 95% viability (as determined by trypan blue exclusion) were used for *in vivo* injections.

Endothelial Cell Isolation

Fresh tissue samples (5 normal ovaries, 7 wound tissues, and 10 epithelial high-grade, stage III or IV invasive serous ovarian cancers) were obtained from patients undergoing primary surgical exploration after approval from the Institutional Review Board. Total RNA from purified endothelial cells was subjected to microarray analysis using the Affymetrix Human U133 plus 2.0 GeneChip platform (Lu et al., 2007).

Real-Time qRT-PCR Validation

Real-time qRT-PCR was performed using 50 ng of total RNA from purified endothelial cells, which were isolated using the RNeasy mini kit (QIAGEN) according to the manufacturer's instructions. cDNA was synthesized from 0.5–1 μg of total RNA using a Verso cDNA kit (Thermo Scientific). qPCR analysis was performed in triplicate using the appropriate primers (Table S2), the SYBR Green ER qPCR SuperMix Universal (Invitrogen, Carlsbad, CA), and Bio-Rad (Bio-Rad Laboratories, Hercules, CA). Relative quantification was calculated using the $2^{-\Delta\Delta CT}$ method normalizing to control for percent fold changes (Donninger et al., 2004).

siRNA Constructs and Delivery

The siRNAs were purchased from Sigma-Aldrich (Woodlands, TX). A non-silencing siRNA that did not share sequence homology with any known human mRNA based on a BLAST search was used as the control for target siRNA. *In vitro* transient transfection was performed as described previously (Landen et al., 2005). Briefly, siRNA (4 μg) was incubated with 10 μL of Lipofectamine 2000 transfection reagent (Lipofectamine) for 20 min at room temperature according to the manufacturer's instructions and added to cells in culture at 80% confluence in 10 cm culture plates.

RPPA and Western Blot Analysis

RF24 and RMG2 cells in the presence or absence of human recombinant EGFL6 protein were subjected to RPPA analysis. Western blot analysis was performed as previously reported (Pradeep et al., 2015; Haemmerle et al., 2017). Cell lysate of RF24 cells were treated with human recombinant EGFL6 protein or anti-EGFL6 antibodies and checked for activation of PI3K and AKT signaling using anti-human EGFL6, PI3K, and AKT antibodies followed by secondary antibodies conjugated with horseradish peroxidase. Experiments were done in duplicate and performed three times.

Phosphorylated RTK Array

A human phosphorylated RTK array kit (R&D Systems) was used to detect the relative tyrosine phosphorylation levels of 42 RTKs in RF24 cells treated with human recombinant EGFL6 protein for 15 min. The human EGFL6 recombinant protein was obtained from Sinobiological (Beijing, China).

Cell Migration Assay

Using Transwell pore Polycarbonate Membrane inserts coated with 0.1% gelatin, we assessed the migration of the RF24 cells in the presence or absence of human *EGFL6* (h*EGFL6*) siRNA. After post-transfection of 48 hr with h*EGFL6*, *integrin*, or *Tie2* siRNAs or after post-transfection of 6 hr with EGFL6 antibody, PI3K inhibitor, or Gly-Arg-Gly-Asp-Ser-Pro (GRGDSP), RF24 cells (1.0×10^5) in MEM serum-free medium were seeded into the upper chamber of the Transwell 0.4 μm pore Polycarbonate Membrane insert (Corning, Lowell, MA). The insert was placed in a 24-well plate containing MEM medium with 15% serum in the lower chamber as chemoattractant. Cells were allowed to migrate in a humidified incubator for 6 hr. Cells that had migrated were stained with hematoxylin and were counted by light microscopy in five random fields (200× original magnification) per sample. Experiments were done in duplicate and performed three times.

Tube Formation Assay

Matrigel (12.5 mg/mL) was thawed at 4°C, and 50 μL was quickly added to each well of a 96-well plate and allowed to solidify for 10 min at 37°C. The wells were then incubated for 6 hr at 37°C with RF24 cells (5,000 per well), which had previously been treated with *EGFL6*, *Integrin β1*, or *Tie2* siRNA (for 48 hr) or EGFL6 antibody, PI3K inhibitor, or GRGDSP (for 6 hr). Experiments were performed in triplicate and repeated twice. Using an Olympus IX81 inverted

Figure 5. EGFL6-Blocking Antibody Reduces Angiogenesis and Tumor Growth

(A) The binding affinity of recombinant EGFL6 to mAbs 93 and 135 was measured by Biacore. The dissociation constant (K_D) value of the mAbs were calculated to be 1.89 nM (mAb 93) and 2.19 nM (mAb 135).

(B) Effect of EGFL6-blocking antibodies on Tie2/AKT activation in RF24 cells (n = 3).

(C) Effect of EGFL6-blocking antibodies on wound healing *in vivo* (n = 5 mice per group, mAb 135, 5 mg/kg).

(D and E) EGFL6 antibodies decreased tube formation (D) and migration (E) of RF24 cells.

(F) Effect of EGFL6-blocking antibodies on tumor weight and tumor nodules in SKOV3ip1 tumor-bearing mice. Seven days after tumor cell injection, mice were randomly divided into three groups (10 mice per group) to receive therapy: (1) control IgG antibody, (2) EGFL6 mAb 93, and (3) EGFL6 mAb 135 (5 mg/kg). Antibody treatment was given once a week.

(G) Effect of targeted EGFL6 on proliferation (Ki67) and microvessel density (CD31). Scale bar, 100 μm. The bars in the graphs correspond sequentially to the labeled columns of images on the left.

Error bars indicates SEM. *$p < 0.05$ versus control IgG. See also Figure S5.

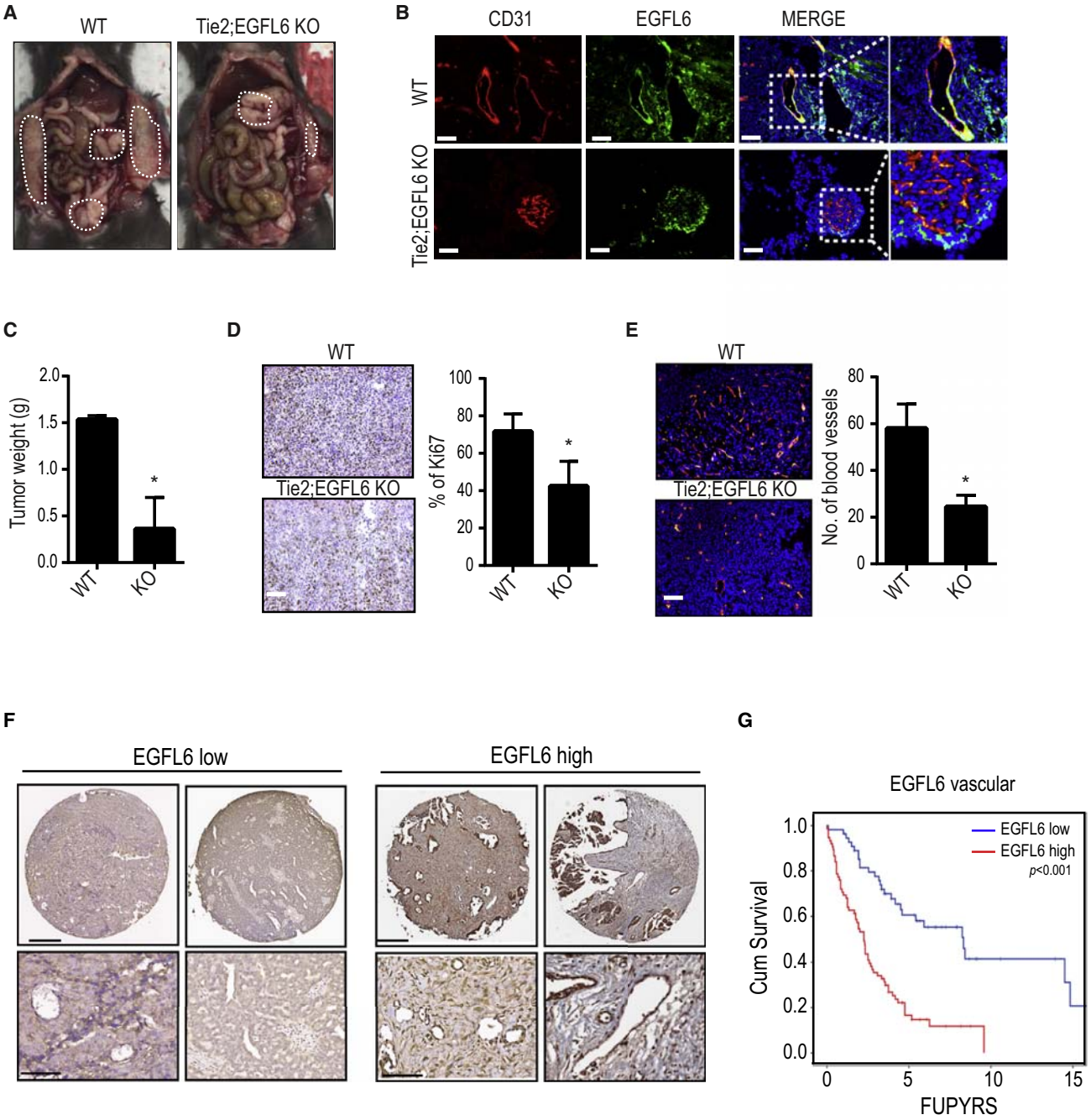

Figure 6. Effect of Endothelial-Specific EGFL6 KO on Tumor Growth and Angiogenesis

(A) Tumor growth in *Tie2;EGFL6* KO mice and WT mice. ID8 murine ovarian cancer cells were injected into KO and WT mice (n = 10 mice per group).

(B) Double immunofluorescence staining of CD31 and EGFL6 in ID8 tumor from WT and KO mice. Scale bar, 100 μm.

(C) Bar graph represents tumor weight.

(D and E) Proliferation (Ki67) (D) and microvessel density (CD31) (E) counted in WT and KO mice tumor sections. Error bars indicate SEM. Scale bar, 100 μm. *$p < 0.05$ versus WT mice.

(F) Representative images of human ovarian cancer vasculature with low or high immunohistochemical staining for EGFL6. Scale bar, 200 μm. Representative images were taken from different samples.

(G) Kaplan-Meier curves of disease-specific mortality of patients whose ovarian vasculature expressed low versus high EGFL6.

See also Figure S6 and Table S1.

microscope, five images per well were taken at 100× magnification. The number of nodes (defined as at least three cells that formed a single point) per image was quantified. To account for cell clumping, the highest and lowest values were removed from each group.

Promoter Analysis and ChIP Assay

RF24 cells were cultured in low-serum medium (0.5% serum) for 18 hr and then treated with EGFL6 (50 ng/mL) for 6 hr. After treatment, ChIP assays were performed using EZ ChIP kit (Millipore, Temecula, CA) as described by the manufacturer. Briefly, cross-linked cells were collected, lysed, sonicated, and subsequently subjected to immunoprecipitation with TWIST1 (Abcam, Cambridge, UK) antibody or immunoglobulin G (IgG) control. Immunocomplexes were collected with protein G agarose beads and eluted. Cross-links were reversed by incubating at 65°C. DNA was then extracted and purified for subsequent PCR amplification using gene-specific primers (Table S2).

Generation of EGFL6 Monoclonal Antibody

Anti-EGFL6 mAbs were identified by screening a large panel of single memory B cells collected from rabbits after immunization with recombinantly expressed *hEGFL6* protein (SinoBiological, Beijing, China). Two lead anti-EGFL6 mAbs (93 and 135) were recombinantly expressed in HEK293 cells (Invitrogen) and purified by use of a protein A resin as we reported previously (Huang et al., 2015; Fan et al., 2015). The purified mAbs were used for this study.

Determination of Antigen Binding Affinity

Binding affinity of the EGFL6 mAbs was determined using the label-free BioLayer Interferometry (BLI) technology (ForteBio, Menlo Park, CA). Briefly, specific biosensors were used to capture the antibody on the sensor, and then the analyte (EGFL6 in a series of concentrations ranging from 55.56 to 0.69 nM) was used to bind to the antibody captured on the biosensor. The binding signal (thickness in nanometers) was monitored continuously to determine the kinetic constants (K_A, association constant; K_D, disassociation constant; K_D (k_{off}/k_{on}), binding affinity) using a 1:1 fitting model with software provided by the manufacturer of the Octet instrument (ForteBio).

Wound Healing Assay

For the *in vivo* assays, on day 0, SKOV3ip1 cancer cells were injected into nude mice, and on day 1, mice were anesthetized with an intraperitoneal injection of ketamine (100 mg/kg). Backs were sterilized with iodine, an excisional wound was made on the mid-dorsal skin with a sterile scissor, and animals were separated into individual cages.

Mice were divided into two groups (n = 10 each). For the treatment of control siRNA-CH and m*EGFL6* siRNA-CH, siRNA treatment was started on day 2 and given twice a week (150 μg/kg), and for antibody treatment, control IgG and EGFL6 antibody were given once weekly (5 mg/kg). The wound was measured every second day (until wound healing was completed). The tumors were harvested when the animals in any group became moribund.

Hindlimb Ischemia

Critical hindlimb ischemia was induced in female nude mice after they were anesthetized with ketamine (100 mg/kg) by intraperitoneal injection. The femoral artery was ligated at its proximal origin as a branch of the external iliac artery to the distal point, where it bifurcates into the saphenous and popliteal arteries. After arterial ligation, the mice were immediately assigned to the following experimental groups (n = 5): control group; ischemia, 24 hr; and ischemia, 96 hr. Color Doppler imaging (VisualSonics FUJIFILM, Toronto, Canada) was performed in three dimensions to monitor blood flow of hindlimbs before and after femoral artery ligation (after 24 and 96 hr) (Krishna et al., 2016). The digital Doppler images were analyzed to assess vascular density in a region from the knee to the toe by calculating the percentage of voxels with Doppler signal above a set threshold indicating blood flow. At each time point, tissue from the ischemic limb was harvested and frozen in optimal cutting temperature compound (OCT) medium. Mouse monoclonal CD31 antibody was used to determine the MVD, and mouse polyclonal EGFL6 antibody was used to determine EGFL6 expression on frozen embedded tissues according to a standard immunostaining procedure (Lu et al., 2010).

Tie2-cre;EGFL6 KO Mice Generation

EGFL6$^{flox/+}$ mice were generated at ingenious Targeting Laboratory (Stony Brook, NY). To selectively delete *EGFL6* in endothelial cells, *Tie2-cre* transgenic mice (males, purchased from the Genetically Engineered Mouse Facility at MD Anderson Cancer Center) were crossed to *EGFL6* floxed mice (females) to generate *Tie2-cre;EGFL6* (males). The *Tie2-cre;EGFL6* males were crossed with *EGFL6* floxed females to obtain the *EGFL6* conditional KO mice. The *Tie2-cre* transgene is known for uniform expression of the cre recombinase in endothelial cells during embryogenesis (Li et al., 2013). Genomic DNA was isolated from tail biopsies of the mouse. *Tie2-cre* transgene and floxed *EGFL6* allele were distinguished by PCR using primers (Table S2).

DATA AND SOFTWARE AVAILABILITY

The accession number for the data reported in this paper is GEO: GSE105437.

SUPPLEMENTAL INFORMATION

Supplemental Information includes six figures and two tables and can be found with this article online at https://doi.org/10.1016/j.celrep.2017.11.020.

AUTHOR CONTRIBUTIONS

A.K.S. and H.-D.H. designed the project. K.N., L.S.M., N.Z., and S.P. designed the experiments. K.N., L.S.M., E.M., S.M., R.R., and M.M.K.S. performed the experimental work. J.L., M.J.B., R.R.B., and G.L.-B. analyzed the results. Z.A., W.X., R.L.C., H.D., and C.V.K. contributed reagents and expertise. K.N., L.S.M., S.P., and A.K.S. wrote the manuscript with input from all co-authors.

ACKNOWLEDGMENTS

Portions of this work were supported by the NIH (CA016672, CA109298, P50 CA217685, P50 CA098258, UH3 TR000943, and R35 CA209904), the Ovarian Cancer Research Fund (Program Project Development Grant), CPRIT (RP150551), the American Cancer Society Research Professor Award, the Blanton-Davis Ovarian Cancer Research Program, the RGK Foundation, and the Frank McGraw Memorial Chair in Cancer Research. K.N. is supported by the KRIBB research initiative program. S.P. is supported by the Liz Tilberis Early Career Award.

Received: December 6, 2016
Revised: September 18, 2017
Accepted: November 2, 2017
Published: December 5, 2017

REFERENCES

Bai, S., Ingram, P., Chen, Y.C., Deng, N., Pearson, A., Niknafs, Y., O'Hayer, P., Wang, Y., Zhang, Z.Y., Boscolo, E., et al. (2016). EGFL6 regulates the asymmetric division, maintenance, and metastasis of ALDH+ ovarian cancer cells. Cancer Res. *76*, 6396–6409.

Bergers, G., and Benjamin, L.E. (2003). Tumorigenesis and the angiogenic switch. Nat. Rev. Cancer *3*, 401–410.

Breier, G. (2000). Angiogenesis in embryonic development—a review. Placenta *21* (*Suppl A*), S11–S15.

Buchner, G., Orfanelli, U., Quaderi, N., Bassi, M.T., Andolfi, G., Ballabio, A., and Franco, B. (2000). Identification of a new EGF-repeat-containing gene from human Xp22: a candidate for developmental disorders. Genomics *65*, 16–23.

Buckanovich, R.J., Sasaroli, D., O'Brien-Jenkins, A., Botbyl, J., Hammond, R., Katsaros, D., Sandaltzopoulos, R., Liotta, L.A., Gimotty, P.A., and Coukos, G. (2007). Tumor vascular proteins as biomarkers in ovarian cancer. J. Clin. Oncol. *25*, 852–861.

Carmeliet, P., and Jain, R.K. (2000). Angiogenesis in cancer and other diseases. Nature *407*, 249–257.

Chim, S.M., Qin, A., Tickner, J., Pavlos, N., Davey, T., Wang, H., Guo, Y., Zheng, M.H., and Xu, J. (2011). EGFL6 promotes endothelial cell migration and angiogenesis through the activation of extracellular signal-regulated kinase. J. Biol. Chem. *286*, 22035–22046.

Chuang, C.Y., Chen, M.K., Hsieh, M.J., Yeh, C.M., Lin, C.W., Yang, W.E., Yang, S.F., and Chou, Y.E. (2017). High level of plasma EGFL6 is associated with clinicopathological characteristics in patients with oral squamous cell carcinoma. Int. J. Med. Sci. *14*, 419–424.

Donninger, H., Bonome, T., Radonovich, M., Pise-Masison, C.A., Brady, J., Shih, J.H., Barrett, J.C., and Birrer, M.J. (2004). Whole genome expression profiling of advance stage papillary serous ovarian cancer reveals activated pathways. Oncogene *23*, 8065–8077.

Eming, S.A., Brachvogel, B., Odorisio, T., and Koch, M. (2007). Regulation of angiogenesis: wound healing as a model. Prog. Histochem. Cytochem. *42*, 115–170.

Fan, X., Brezski, R.J., Deng, H., Dhupkar, P.M., Shi, Y., Gonzalez, A., Zhang, S., Rycyzyn, M., Strohl, W.R., Jordan, R.E., et al. (2015). A novel therapeutic strategy to rescue the immune effector function of proteolytically inactivated cancer therapeutic antibodies. Mol. Cancer Ther. *14*, 681–691.

Ferrara, N., and Kerbel, R.S. (2005). Angiogenesis as a therapeutic target. Nature *438*, 967–974.

Gressett, S.M., and Shah, S.R. (2009). Intricacies of bevacizumab-induced toxicities and their management. Ann. Pharmacother. *43*, 490–501.

Haemmerle, M., Taylor, M.L., Gutschner, T., Pradeep, S., Cho, M.S., Sheng, J., Lyons, Y.M., Nagaraja, A.S., Dood, R.L., Wen, Y., et al. (2017). Platelets reduce anoikis and promote metastasis by activating YAP1 signaling. Nat. Commun. *8*, 310.

Huang, Z., Choi, B.K., Mujoo, K., Fan, X., Fa, M., Mukherjee, S., Owiti, N., Zhang, N., and An, Z. (2015). The E3 ubiquitin ligase NEDD4 negatively regulates HER3/ErbB3 level and signaling. Oncogene *34*, 1105–1115.

Koskas, M., Chereau, E., Ballester, M., Selle, F., Rouzier, R., and Daraï, E. (2010). Wound complications after bevacizumab treatment in patients operated on for ovarian cancer. Anticancer Res. *30*, 4743–4747.

Krishna, S.M., Omer, S.M., and Golledge, J. (2016). Evaluation of the clinical relevance and limitations of current pre-clinical models of peripheral artery disease. Clin. Sci. *130*, 127–150.

Krzeszinski, J.Y., Wei, W., Huynh, H., Jin, Z., Wang, X., Chang, T.C., Xie, X.J., He, L., Mangala, L.S., Lopez-Berestein, G., et al. (2014). miR-34a blocks osteoporosis and bone metastasis by inhibiting osteoclastogenesis and Tgif2. Nature *512*, 431–435.

Landen, C.N., Jr., Chavez-Reyes, A., Bucana, C., Schmandt, R., Deavers, M.T., Lopez-Berestein, G., and Sood, A.K. (2005). Therapeutic EphA2 gene targeting in vivo using neutral liposomal small interfering RNA delivery. Cancer Res. *65*, 6910–6918.

Langley, R.R., Ramirez, K.M., Tsan, R.Z., Van Arsdall, M., Nilsson, M.B., and Fidler, I.J. (2003). Tissue-specific microvascular endothelial cell lines from H-2K(b)-tsA58 mice for studies of angiogenesis and metastasis. Cancer Res. *63*, 2971–2976.

Li, S., Haigh, K., Haigh, J.J., and Vasudevan, A. (2013). Endothelial VEGF sculpts cortical cytoarchitecture. J. Neurosci. *33*, 14809–14815.

Lu, C., Bonome, T., Li, Y., Kamat, A.A., Han, L.Y., Schmandt, R., Coleman, R.L., Gershenson, D.M., Jaffe, R.B., Birrer, M.J., and Sood, A.K. (2007). Gene alterations identified by expression profiling in tumor-associated endothelial cells from invasive ovarian carcinoma. Cancer Res. *67*, 1757–1768.

Lu, C., Han, H.D., Mangala, L.S., Ali-Fehmi, R., Newton, C.S., Ozbun, L., Armaiz-Pena, G.N., Hu, W., Stone, R.L., Munkarah, A., et al. (2010). Regulation of tumor angiogenesis by EZH2. Cancer Cell *18*, 185–197.

Masiero, M., Simões, F.C., Han, H.D., Snell, C., Peterkin, T., Bridges, E., Mangala, L.S., Wu, S.Y., Pradeep, S., Li, D., et al. (2013). A core human primary tumor angiogenesis signature identifies the endothelial orphan receptor ELTD1 as a key regulator of angiogenesis. Cancer Cell *24*, 229–241.

Nichol, D., and Stuhlmann, H. (2012). EGFL7: a unique angiogenic signaling factor in vascular development and disease. Blood *119*, 1345–1352.

Oberauer, R., Rist, W., Lenter, M.C., Hamilton, B.S., and Neubauer, H. (2010). EGFL6 is increasingly expressed in human obesity and promotes proliferation of adipose tissue-derived stromal vascular cells. Mol. Cell. Biochem. *343*, 257–269.

Peng, J., Ramesh, G., Sun, L., and Dong, Z. (2012). Impaired wound healing in hypoxic renal tubular cells: roles of hypoxia-inducible factor-1 and glycogen synthase kinase 3β/β-catenin signaling. J. Pharmacol. Exp. Ther. *340*, 176–184.

Pradeep, S., Huang, J., Mora, E.M., Nick, A.M., Cho, M.S., Wu, S.Y., Noh, K., Pecot, C.V., Rupaimoole, R., Stein, M.A., et al. (2015). Erythropoietin stimulates tumor growth via EphB4. Cancer Cell *28*, 610–622.

Schäfer, M., and Werner, S. (2008). Cancer as an overhealing wound: an old hypothesis revisited. Nat. Rev. Mol. Cell Biol. *9*, 628–638.

Schmidt, M., Paes, K., De Mazière, A., Smyczek, T., Yang, S., Gray, A., French, D., Kasman, I., Klumperman, J., Rice, D.S., and Ye, W. (2007). EGFL7 regulates the collective migration of endothelial cells by restricting their spatial distribution. Development *134*, 2913–2923.

Shord, S.S., Bressler, L.R., Tierney, L.A., Cuellar, S., and George, A. (2009). Understanding and managing the possible adverse effects associated with bevacizumab. Am. J. Health Syst. Pharm. *66*, 999–1013.

Tonnesen, M.G., Feng, X., and Clark, R.A. (2000). Angiogenesis in wound healing. J. Investig. Dermatol. Symp. Proc. *5*, 40–46.

Wang, X., Gong, Y., Wang, D., Xie, Q., Zheng, M., Zhou, Y., Li, Q., Yang, Z., Tang, H., Li, Y., et al. (2012). Analysis of gene expression profiling in meningioma: deregulated signaling pathways associated with meningioma and EGFL6 overexpression in benign meningioma tissue and serum. PLoS ONE *7*, e52707.

Witte, L., Hicklin, D.J., Zhu, Z., Pytowski, B., Kotanides, H., Rockwell, P., and Böhlen, P. (1998). Monoclonal antibodies targeting the VEGF receptor-2 (Flk1/KDR) as an anti-angiogenic therapeutic strategy. Cancer Metastasis Rev. *17*, 155–161.

Yeung, G., Mulero, J.J., Berntsen, R.P., Loeb, D.B., Drmanac, R., and Ford, J.E. (1999). Cloning of a novel epidermal growth factor repeat containing gene EGFL6: expressed in tumor and fetal tissues. Genomics *62*, 304–307.

Zhu, Z., Rockwell, P., Lu, D., Kotanides, H., Pytowski, B., Hicklin, D.J., Bohlen, P., and Witte, L. (1998). Inhibition of vascular endothelial growth factor-induced receptor activation with anti-kinase insert domain-containing receptor single-chain antibodies from a phage display library. Cancer Res. *58*, 3209–3214.